Supporting Information

Single Ensemble Nonexponential Photoluminescent Population Decays from a Broadband White-Light-Emitting Perovskite

Joseph E. Thomaz[1], Kurt P. Lindquist[1], Hemamala I. Karunadasa[#,1,2], and Michael D. Fayer*[,1]

1. Department of Chemistry, Stanford University, Stanford, CA 94305
2. Stanford Institute for Materials and Energy Sciences, SLAC National Accelerator Laboratory, Menlo Park, California 94025, USA
[#]Email: hemamala@stanford.edu, Phone: 650 723-0288
*Email: fayer@stanford.edu, Phone: 650 723-4446

Time-Resolved Emission Spectra Methodology

Construction of time-resolved emission spectra is a data processing technique that can be implemented in optical spectroscopy to study photochemical systems.[1] This method involves the collection of a large number of population decays across the emission spectrum. Each decay is acquired for the same amount of time under identical experimental conditions to maintain the correct relative amplitude across the emission band. By taking data points from the collected decays at a specific time, the emission spectrum at that time can be constructed. This method has been successfully used to study proton transport,[2-5] as well as solvation dynamics.[6-9] While TCSPC has been used previously to study white-light emitting perovskites,[10] it has only been used by measuring population decays at a few wavelengths and fitting each decay individually. Generation of the time-resolved emission spectra requires the collection of many more population decays, but in return provides much greater detail about the chemical system.

Time-dependent emission spectra can be constructed by stepping a monochromator across the emission spectrum and collecting luminescent decays at a large number of wavelengths, each for the same amount of time under exactly the same experimental conditions. Unlike the time-independent spectra where each emission wavelength is time-integrated, comparable to the steady state spectrum, a spectrum at a particular time is generated by plotting

the intensity of each luminescent decay at the single time point. Then spectra are obtained for many time points. By normalizing each spectrum, the emission line shape can be determined as a function of time without the effects of population decay.

Instrument Response

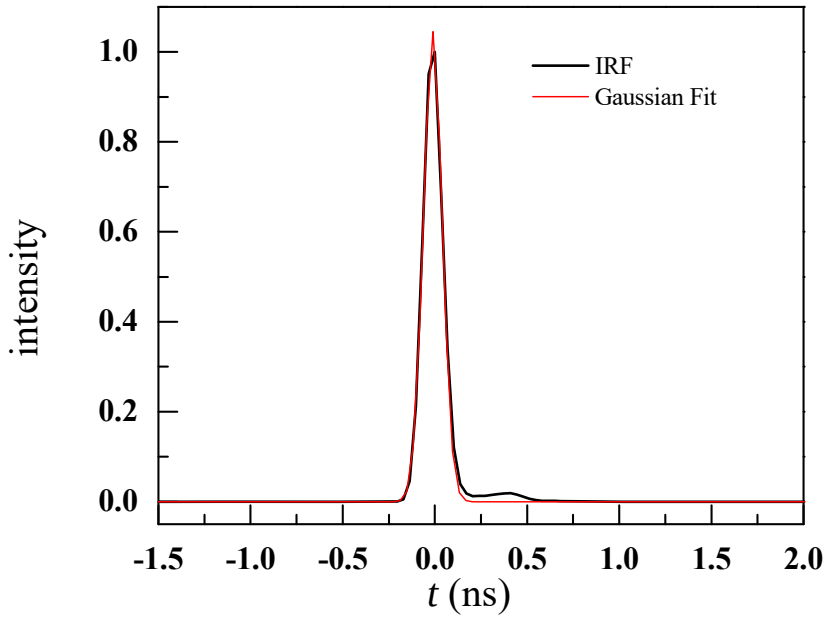

Figure S1: The instrument response of the TCSPSC setup. There is a Gaussian fit with a FWHM of 120 ps.

Polarization Considerations

Photoluminescent decays were collected across the emission window in both horizontal and vertical polarizations in the lab frame under identical experimental conditions. The luminescent photons were resolved through a fixed polarizer with horizontal polarization. The (EDBE)$PbBr_4$ crystal grows as a rectangular plate with the inorganic sheets stacking along the crystallographic *b*-axis, and the inorganic layers propagating along the crystallographic *ac* plane. The plate-like crystal was always mounted in the sample cell such that the longest dimension of the crystal, corresponding to the crystallographic *c*-axis, was along the horizontal axis in the lab

frame, while the *a*-axis was along the vertical axis in the lab frame. The shortest dimension of the crystal corresponded to the crystallographic *b*-axis. One of the concerns regarding polarization in TCSPC experiments is the separation of orientational dynamics from the excited state population dynamics. A significant number of TCSPC experiments consist of fluorescent probe molecules dissolved in a liquid.[43-45] In liquids, the probes can undergo orientational relaxation following excitation, contributing an orientational relaxation time dependence to the emission. The magic angle polarization can be used to eliminate the contributions of orientational relaxation from the detected emission decay. In a perovskite crystal, however, magic angle polarization is unnecessary as there is no orientational relaxation. In the perovskite crystals, the spectrum and dynamics are independent of polarization, but there is a polarization-dependence in the emission intensity detected through the horizontal polarizer. Far more luminescent photons are detected when the excitation is vertically polarized (along the *ab* plane) compared to horizontally polarized (along the *bc* plane). Therefore, the absorption transition dipole is stronger along the *a*-axis compared to the *c* axis of the crystal. An examination of the crystal structure explains this anisotropy: continuous Br−Pb−Br connectivity (bond angle of 173°) is evident along the *a* axis, whereas the connectivity along the *c* axis is disrupted due to the corrugation of the (110) perovskite sheets.

Macroscopic Defects in (EDBE)$PbBr_4$

In general, fluorometers use an arc lamp source. The light impinges on a grating to select the excitation wavelength. This results in a relatively large excitation stripe, which does not permit location specificity. The laser used in this study, however, has diameter of 1 millimeter (99% of the intensity). This is small enough, relative to the size of the crystals, that

spectroscopic data can be collected at a large number of distinct locations across the face of the crystal.

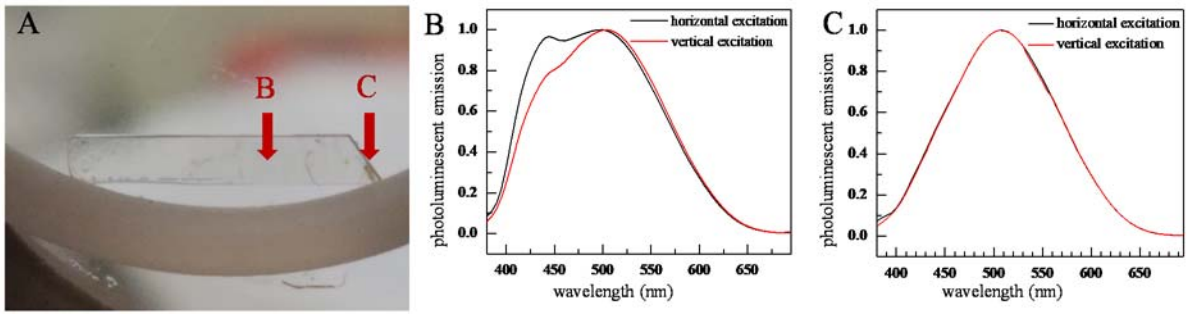

Figure S2: (A) A photo of one of the (EDBE)$PbBr_4$ crystals used in this experiment mounted in a sample cell resting on a 1 mm Teflon spacer. The relatively small spot size of the laser permitted the study of a number of sites on the crystal. Note that the crystal is mounted such that the long-axis is horizontal (B) Time-integrated spectra taken with vertical and horizontal excitation polarizations, but on a crystal site with a visible impurity seen in panel A. The presence of a previously reported side peak is evident. At this site, a clear polarization-dependence because the transition dipoles from the species generating each of the two peak are not aligned. (C) Time-integrated spectra taken with vertical and horizontal polarizations. There are very little, if any, polarization effects at this site. This panel is representative of what was observed on the vast majority of crystal sites.

Figure S2A is an image of an (EDBE)$PbBr_4$ crystal used in this study mounted on a sample cell. (The results presented here were reproduced by measurements on another crystal.) It is resting on top of a one quarter of one millimeter thick Teflon ring. Spectra were taken on 15 distinct spots across the crystal. Of these spots, 14 showed essentially identical spectra as displayed in Figure S2B with no polarization-dependence other than intensity. The last spot displayed in Figure S2C, however, generates a very different spectrum with a very clear polarization-dependence. The most significant difference between panels B and C is the presence of a narrow side peak in the latter centered near 440 nm. Figure S2A shows the spot, labeled C, which gave the spectrum seen in Figure S2C. In the photograph, there is a distinct spot, which to the eye appears brown-colored. The visible difference in region C is associated with the observed side peak. The polarization-dependence demonstrates that the absorption and/or emission transition dipoles of the two emission bands in the defective region do not lie on the same axis.

The presence of the additional peak centered at ~440 nm shown in Figure S2C only in the defective crystal region is important because previous studies reported steady state spectra of broadband white-light-emitting perovskites showing the presence of this side peak at 440 nm in powder samples,[11] but it was much smaller than the side peak seen in Figure S2C. In the case of crystal samples, this is likely due to the large spot size of the fluorometer. Because the spot size encompasses a significant portion of the crystal, locations with and without defective regions contribute to the steady-state spectrum resulting in a plot that is a linear combination of Figures 2B and 2C. In the case of thin film and powder samples, the domain sizes are much smaller making it very difficult to visually identify a defective spot. Even when ultrafast data are taken, thin film and powder samples still show the presence of the 440 nm side peak suggesting that the impurity or defect is present.

Population Decays Normalized at 15 ns

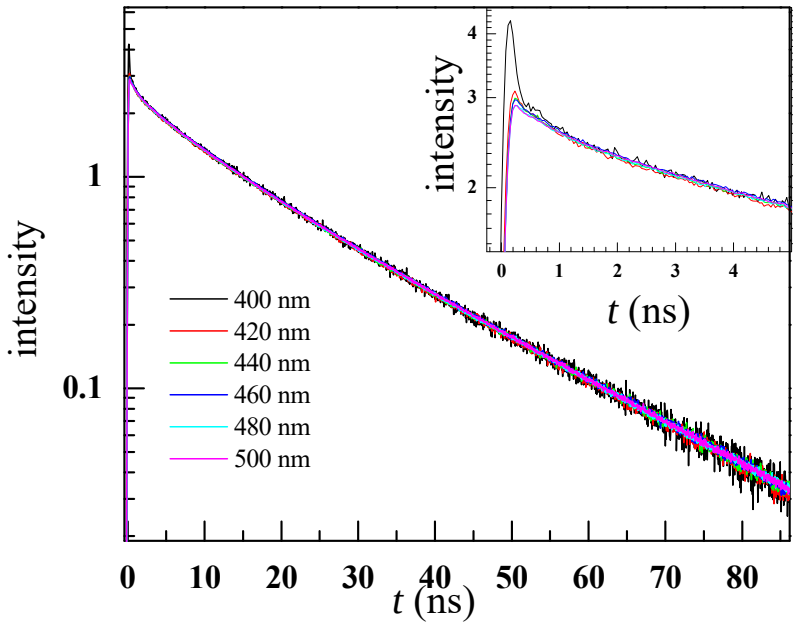

Figure S3: The luminescent decays of (EDBE)$PbBr_4$ at various emission wavelengths each normalized to their value at 15 ns. The inset shows the first 5 ns of the decay. All emission wavelengths have the same behavior after ~400 ps.

Fits to Integrated Population Decays

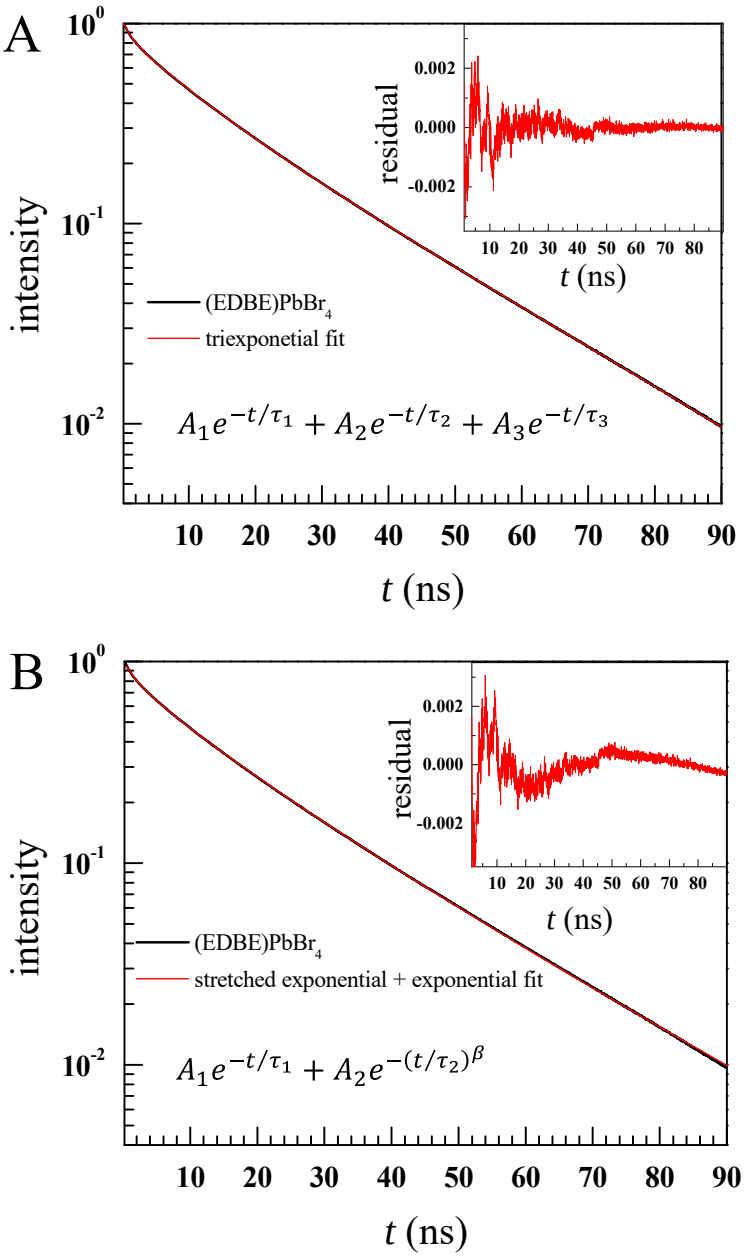

Figure S4: (A) Fits to a triexponential to the (EDBE)$PbBr_4$ integrated population decay. (B) Fits to a single exponential plus a stretched exponential to the (EDBE)$PbBr_4$ integrated population decay.

The Akaike Information Criterion (AIC), a statistical test used to judge the efficacy of fitting functions, was employed to compare the quality of the two fitting functions.[34] AIC compares the quality of fits to a data set using two fitting functions. AIC takes into account differences in the number of adjustable parameters. While the fits appear virtually identical, AIC demonstrates that the tri-exponential decay is the appropriate fitting function.

References

(1) Koti, A.; Krishna, M.; Periasamy, N. Time-Resolved Area-Normalized Emission Spectroscopy (TRANES): A Novel Method for Confirming Emission from Two Excited States. *J. Phys. Chem. A* **2001**, *105*, 1767-1771.

(2) Lawler, C.; Fayer, M. D. Proton Transfer in Ionic and Neutral Reverse Micelles. *J. Phys. Chem. B* **2015**, *119*, 6024-6034.

(3) Nandi, N.; Sahu, K. Analysis of Excited State Proton Transfer Dynamics of Hpts in Methanol-Water Mixtures from Time-Resolved Area-Normalised Emission Spectrum (TRANES). *J. Photochem. Photobio. A* **2019**, *374*, 138-144.

(4) Singh, S.; Koley, S.; Mishra, K.; Ghosh, S. An Approach to a Model Free Analysis of Excited-State Proton Transfer Kinetics in a Reverse Micelle. *J. Phys. Chem. C* **2018**, *122*, 732-740.

(5) Fujii, K.; Yasaka, Y.; Ueno, M.; Koyanagi, Y.; Kasuga, S.; Matano, Y.; Kimura, Y. Excited-State Proton Transfer of Cyanonaphthols in Protic Ionic Liquids: Appearance of a New Fluorescent Species. *J. Phys. Chem. B* **2017**, *121*, 6042-6049.

(6) Thomaz, J. E.; Bailey, H. E.; Fayer, M. D. The Influence of Mesoscopic Confinement on the Dynamics of Imidazolium-Based Room Temperature Ionic Liquids in Polyether Sulfone Membranes. *J. Chem. Phys.* **2017**, *147*, 194502.

(7) Maroncelli, M.; Zhang, X.-X.; Liang, M.; Roy, D.; Ernsting, N. P. Measurements of the Complete Solvation Response of Coumarin 153 in Ionic Liquids and the Accuracy of Simple Dielectric Continuum Predictions. *Faraday Discuss.* **2012**, *154*, 409-424.

(8) Karmakar, R.; Samanta, A. Solvation Dynamics of Coumarin-153 in a Room-Temperature Ionic Liquid. *J. Phys. Chem. A* **2002**, *106*, 4447-4452.

(9) Pant, D.; Levinger, N. E. Dynamics of Polar Solvation at the Surface of a ZrO2 Nanoparticle. *Chem. Phys. Lett.* **1998**, *292*, 200-206.

(10) Hu, T.; Smith, M. D.; Dohner, E. R.; Sher, M.-J.; Wu, X.; Trinh, M. T.; Fisher, A.; Corbett, J.; Zhu, X.-Y.; Karunadasa, H. I. Mechanism for Broadband White-Light Emission from Two-Dimensional (110) Hybrid Perovskites. *J. Phys. Chem. Lett.* **2016**, *7*, 2258-2263.